DOI: 10.1021/ma100236u

Macromolecules
ARTICLE

Crystal Orientation of Poly(ε-caprolactone) Homopolymers Confined in Cylindrical Nanodomains

Shuichi Nojima,*,† Yuya Ohguma,† Ken-ichi Kadena,† Takashi Ishizone,† Yuta Iwasaki,‡ and Kazuo Yamaguchi‡,§

†*Department of Organic and Polymeric Materials, Graduate School of Science and Engineering, Tokyo Institute of Technology, H-125, 2-12-1 Ookayama Meguro-Ku, Tokyo 152-8552, Japan,* ‡*Department of Chemistry, Faculty of Science, Kanagawa University, Hiratsuka, Kanagawa 259-1293, Japan, and* §*Research Institute for Photofunctionalized Materials, Kanagawa University, Hiratsuka, Kanagawa 259-1293, Japan*

Received January 30, 2010; Revised Manuscript Received March 22, 2010

ABSTRACT: The crystal orientation of poly(ε-caprolactone) (PCL) homopolymers, spatially confined in cylindrical nanodomains surrounded by polystyrene (PS) matrices, has been investigated as a function of crystallization temperature T_c (-60 °C ≤ T_c ≤ -40 °C) using two-dimensional small-angle X-ray scattering (2D-SAXS) and wide-angle X-ray diffraction (2D-WAXD). The sample was prepared by microphase separation of an PCL-*block*-PS copolymer followed by photocleavage at the block junction between PCL and PS blocks. The results were compared with crystal orientation of PCL blocks before photocleavage, *i.e.*, PCL chains with one chain-end tethered at the cylinder interface. The lamellar crystals of PCL homopolymers and PCL blocks were preferentially oriented in cylindrical nanodomains irrespective of T_c, *i.e.*, the *b* axis of crystal unit cells was oriented parallel to the long axis of cylinders. The degree of crystal orientation increased remarkably with increasing T_c for PCL homopolymers, whereas it improved slightly for PCL blocks, yielding a large difference in the degree of crystal orientation between two systems at higher T_c (≥ -45 °C).

1. Introduction

Crystallization of long chains confined in isolated nanodomains (*i.e.*, cylinders and spheres) is an interesting research subject from the viewpoint of polymer nanotechnology. Crystalline−amorphous diblock copolymers form a variety of microdomain structures in the melt depending on composition, and therefore it is possible to investigate the crystallization behavior of confined blocks. Many experimental results reported so far indicate that the spatial confinement considerably affects the crystallization behavior, yielding a large reduction in crystallinity and crystallizable temperature.[1−12] In addition, the lamellar crystals formed in nanodomains show characteristic orientation when compared with those in bulk homopolymers without any spatial confinement. For example, when the block chain crystallizes in cylindrical nanodomains (*nanocylinders*), the stem direction in the lamellar crystals (*c* axis of crystal unit cells) is reported to significantly depend on crystallization temperature T_c;[13−16] the *c* axis is almost random at lower T_c, while it is perpendicular against the cylinder axis at higher T_c.

When we study the crystallization of block chains confined in nanocylinders (Figure 1a), we can consider two principal factors which simultaneously affect the crystallization mechanism: (1) spatial confinement by accommodating the crystalline blocks in nanocylinders and (2) chain confinement by tethering the blocks at the cylinder interface. To understand the effects of two factors separately on crystallization it is necessary to prepare such a system where *crystalline homopolymers* are confined in nanocylinders (Figure 1b) and to investigate the difference in the crystallization behavior and resulting morphology between two systems.

Crystal orientation of homopolymers confined in nanocylinders has been recently investigated using nanorods existing in anodic aluminum oxide (AAO).[17−20] These results revealed a variety of crystallization processes depending on the cylinder diameter, crystallization temperature, and chain mobility within the cylinders. The crystallization behavior of homopolymers confined in isolated nanodomains was also predicted using computer simulation.[21−24] We have recently investigated the crystallization process of poly(δ-valerolactone) (PVL) homopolymers confined in spherical or cylindrical nanodomains[25] originally formed by microphase separation of PVL-*block*-polystyrene (PVL-*b*-PS) diblocks, and compared the crystallization rate of PVL homopolymers with that of PVL blocks, *i.e.*, PVL with one-chain end tethered at the nanodomain interface. We found that the initial crystallization rate of PVL blocks was significantly higher than that of PVL homopolymers, which will arise from the nucleation effect at the tethering point of PVL blocks. However, the final crystallinity of PVL homopolymers was moderately higher than that of PVL blocks owing to the less restriction of chain conformation.

In this study, we aim to clarify the difference in crystal orientation between homopolymers and block chains both confined in the nanocylinder (Figure 1). The samples were prepared by microphase separation of a poly(ε-caprolactone)-*block*-polystyrene (PCL-*b*-PS) diblock copolymer followed by photocleavage at the junction point between PCL and PS blocks. As a result, we prepared two systems, *i.e.*, PCL homopolymers and PCL blocks with the same molecular weight both confined in the nanocylinders with identical geometry. First, we applied a rotational shear to the sample to get preferential orientation of nanocylinders, which was confirmed using two-dimensional small-angle X-ray scattering (2D-SAXS). Next, PCL crystal orientation against the cylinder axis was investigated for both systems as a function of crystallization temperature T_c (-60 °C ≤ T_c ≤ -40 °C) using 2D wide-angle X-ray diffraction (2D-WAXD). Finally, we discussed the difference in the crystallization mechanism between two systems.

*Corresponding author. Telephone: +81-3-5734-2132. Fax: +81-3-5734-2888. E-mail:snojima@polymer.titech.ac.jp.

 Published on Web 04/01/2010

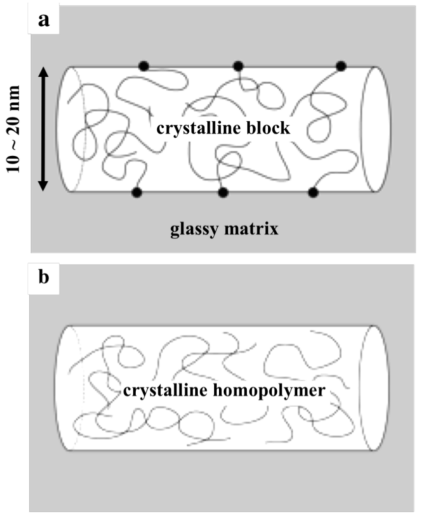

Figure 1. Schematic illustration showing crystalline blocks (a) and crystalline homopolymers (b) both confined in a nanocylinder.

2. Experimental Section

2.1. Samples. The block copolymer used in this study is poly(ε-caprolactone)-*block*- polystyrene (PCL-*b*-PS) with a photocleavable *o*-nitrobenzyl group [26] between PCL and PS blocks (Scheme 1). The detailed method of sample synthesis will soon appear. The result of molecular characterization is shown in Table 1, where "PCL−PS" in the sample code represents the normal diblock copolymer before photocleavage, while "PCL/PS" represents the sample after photocleavage, i.e., PCL homopolymers confined in PS matrices. The SAXS and TEM results described below (Figures 2b and 2c) indicate that PCL−PS forms a cylindrical microdomain structure in the melt. The glass transition temperature of PS blocks is ca. 100 °C and the melting temperature of PCL blocks is *ca.* 40 °C (Figure 2a), so that vitrification of PS chains will prevent macrophase separation between PCL and PS homopolymers after photocleavage, and eventually we can get PCL homopolymers confined in nanocylinders surrounded by PS matrices originally provided by microphase separation of PCL−PS. It should be noted that the melting temperature of PCL homopolymers is slightly higher than that of PCL blocks, which was also found in our previous study.[25]

The following specific volumes were used to calculate the volume fraction of each block from ^{1}H NMR results. For polystyrene (above T_g),[27]

$$v_{sp}(T) = 0.9217 + 5.412 \times 10^{-4} \times T + 1.687 \times 10^{-7} \times T^2 \quad (1)$$

and for amorphous poly(ε-caprolactone)[28]

$$v_{sp}(T) = 0.9106 + 6.013 \times 10^{-4} \times T \quad (2)$$

where $v_{sp}(T)$ is in cubic centimeters per gram and T is in degrees Celsius.

2.2. Orientation of Nanocylinders. A disk sample of PCL−PS with the diameter of ca. 20 mm and the thickness of ca. 0.9 mm was subject to the rotational shear at 120 °C under a dry nitrogen atmosphere using Linkam shearing cell (CSS-450). The angular velocity applied was 3.14 rad/s, which corresponded to the shear rate of 35 s^{-1}. After cooling the sample into room temperature, the specimen for 2D-SAXS and 2D-WAXD experiments was cut out from the disk. The 2D-SAXS results revealed that the nanocylinders were preferentially oriented parallel to the shear direction (Figure 3).

2.3. Photocleavage. UV with 10 W/cm^2 in intensity and wavelength longer than 300 nm (USHIO Optical Modulex, USH-500SC) was irradiated to the sample with the thickness of ca. 0.9 mm to cleave the *o*-nitrobenzyl group inserted between PCL and PS blocks (Scheme 1). This photocleaving process is completely irreversible, that is, once the block junction is broken it never recombines into the copolymer. The samples before and after UV irradiation were examined using gel permeation chromatography (GPC), and the photocleavage yield was evaluated from the ratio of GPC peak areas for PCL−PS and PS homopolymer. The yield depended significantly on the UV irradiation time t_{UV}, and the maximum yield was *ca.* 80% at $t_{UV} \geq 20$ h. This fact does not imply that the system has two nanocylinders, one consisting of pure PCL homopolymers and the other PCL blocks, but the uncleaved PCL blocks will be uniformly distributed in every nanocylinder because the DSC curve showed a single endothermic peak during heating (Figure 2a). Therefore, we can expect the effect of chain tethering at the interface on crystal orientation using PCL blocks and PCL homopolymers both confined in the nanocylinders with identical geometry.

2.4. Differential Scanning Calorimetry (DSC) Measurements. A Perkin-Elmer DSC Diamond was used with a heating rate of 20 °C/min to obtain the melting temperature of PCL chains and the glass transition temperature of PS chains in PCL−PS and PCL/PS both crystallized at −60 °C for 4 h. The temperature range where the PCL chains could crystallize was also checked using DSC with a constant cooling rate (= −10 °C/min), and it was found to be extremely low (≤ −40 °C) compared with that of PCL homopolymers without spatial confinement (≤ 50 °C).

2.5. Transmission Electron Microscope (TEM). The morphology formed in PCL−PS was observed using TEM (JEOL model 200CX with an acceleration voltage of 100 kV). The sample crystallized at −60 °C for 4 h was exposed to RuO_4 vapor at room temperature for 24 h to give the contrast and also to fix the morphology, then microtomed into a sliver with ca. 60 nm in thickness, and finally the sliver was again exposed to RuO_4 vapor for 1 h at room temperature. RuO_4 diffuses easily into the amorphous region in the sample (PS blocks and uncrystallized PCL blocks) to present dark contrast, whereas the PCL crystal shows bright contrast owing to slow diffusion of RuO_4.[29]

2.6. One-Dimensional Small-Angle X-ray Scattering (1D-SAXS) Measurements. The morphology formed in PCL−PS before orientation was investigated using synchrotron small-angle X-ray scattering (SR-SAXS), which was performed at Photon Factory in High Energy Accelerator Research Organization, Tsukuba, Japan, with a small-angle X-ray equipment for solution installed at beamline BL-10C. Details of the equipment and the instrumentation are described in our previous publications.[30−33] The scattered intensity was recorded with a one-dimensional position-sensitive proportional counter (PSPC), by which isotropic scattering from the sample was obtained as a function of s (= $(2/\lambda)[\sin\theta]$; λ, X-ray wavelength (= 0.1488 nm); 2θ, scattering angle). The long period, *i.e.*, an alternating distance of the morphology, was evaluated from the angular position of the primary intensity peak, and finally the diameter of PCL nanocylinders was calculated from the long period and the volume fraction of PCL blocks in the system.

2.7. Two-Dimensional SAXS (2D-SAXS) and Wide-Angle X-ray Diffraction (2D-WAXD) Measurements. 2D-SAXS and 2D-WAXD measurements were performed using a Rigaku NanoViewer with a rotating-anode X-ray generator operating at 45 kV and 60 mA. The wavelength used was 0.1542 nm of CuKα radiation. The detector was an image plate (FUJI Film BAS-SR 127) with the size of 10 × 10 cm^2, and the accumulation time was 6−12 h. The WAXD intensity at selected diffraction angles was plotted as a function of azimuthal angle ϕ after subtracting the background scattering to evaluate the degree of crystal orientation f. The method to evaluate f is precisely described in section 3.3.

3. Results and Discussion

3.1. Characterization of PCL−PS and Orientation of Nanocylinders. Figure 2a shows the DSC heating thermogram of PCL−PS isothermally crystallized at −60 °C for 4 h. The melting endothermic peak of PCL blocks appears at *ca.*

Scheme 1. Photocleavage Reaction

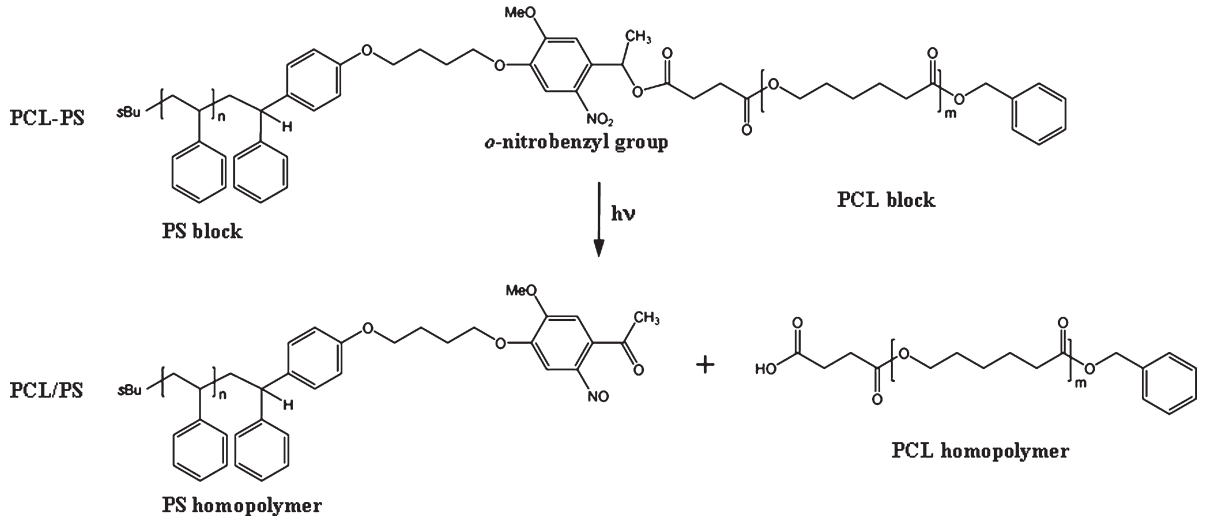

Table 1. Molecular Characteristics of PCL-*b*-PS Used in This Study

sample code	M_n of PCL blocks[a](g/mol)	M_n of PS blocks[a] (g/mol)	total M_n[a]	M_w/M_n[b]	PCL:PS(vol %)	$T_{m,PCL}$[c](°C)	$T_{g,PS}$[c](°C)	morphology[d]	D[e] (nm)	p[f] (%)
PCL−PS	7900	24 100	32 000	1.05	25:75	40	100	cylinder	13.0	0
PCL/PS	7900	24 100	32 000	1.05	25:75	45	100	cylinder	13.0	80

[a] Determined by ^{1}H NMR. [b] Determined by GPC. [c] Determined by DSC. [d] Evaluated from 1D-SAXS and TEM. [e] Calculated from the long period and the volume fraction of PCL blocks. [f] Maximum photocleavage yield obtained by GPC.

40 °C (= $T_{m,PCL}$) and the change in the baseline due to glass transition of PS blocks (indicated by an arrow) at ca. 100 °C (= $T_{g,PS}$). We can expect from Figure 2a that vitrification of PS chains prevents macrophase separation between photocleaved PCL and PS homopolymers in the temperature range below $T_{g,PS}$. Therefore, it is possible to crystallize and melt PCL homopolymers repeatedly within the nanodomain originally formed by microphase separation of PCL−PS. In fact, PCL/PS was transparent as far as it was treated at T < 70 °C, suggesting no macrophase separation between PCL and PS homopolymers.

Figure 2b shows the 1D-SAXS curves measured at room temperature for PCL−PS crystallized at -60 °C for 4 h and amorphous PCL−PS before crystallization. The SAXS curve of crystallized PCL−PS has several scattering peaks, the angular positions of which exactly correspond to a ratio of 1:$\sqrt{3}$:$\sqrt{4}$:$\sqrt{7}$, indicating the formation of cylindrical microdomains. The higher-order peaks cannot be observed in the SAXS curve of amorphous PCL−PS, which is ascribed to the small difference in electron density between amorphous PS (332 e/nm^3 below 100 °C[27]) and amorphous PCL (354 e/nm^3 at 25 °C[28]). However, it is found from Figure 2b that the primary peak position does not change substantially before and after crystallization of PCL blocks, suggesting that the cylindrical microdomain structure is completely preserved after crystallization (confined crystallization). This crystallization behavior has been investigated for several crystalline−amorphous diblocks with $T_g > T_c$ (T_g, glass transition temperature of amorphous blocks; T_c, crystallizable temperature of crystalline blocks),[34,35] where crystallization does not bring about the morphological transition (microdomain structure → crystallized lamellar morphology) owing to the glassy matrix. On the basis of the volume fraction of PCL blocks in the system (= 0.25 in Table 1) and the primary peak position in the SAXS curve, the diameter of nanocylinders is estimated to be 13.0 nm, which is smaller than that of poly(δ-valerolactone)-*block*-PS (PVL-*b*-PS) investigated in our previous study (= 15.7 nm).[25] This difference will lead to the reduced crystallinity of PCL blocks and PCL homopolymers compared with that of PVL chains owing to the narrower confined space, as discussed later.

Figure 2c shows the TEM picture of PCL−PS crystallized at −60 °C for 4 h. We can observe the hexagonally arranged white spheres at the left region of Figure 2c and also alternating lamellar structure at the right, indicating that PCL−PS forms the cylindrical microdomain structure with the PCL cylinder and PS matrix. The two geometries (spheres and lamellae) simply arise from the difference in the cutting direction of nanocylinders. Therefore, the TEM result is consistent with the SAXS result described above. The diameter of nanocylinders evaluated from Figure 2c is ca. 11 nm, which agrees satisfactorily with that obtained from SAXS measurements (= 13.0 nm).

Uniaxial orientation of nanocylinders was carried out before photocleavage at 120 °C by applying the rotational shear, as described in the Experimental Section. Parts a−c of Figure 3 show the 2D-SAXS patterns observed from X, Y, and Z directions for PCL−PS crystallized at −60 °C for 4 h, where Z represents the shear direction and X and Y are perpendicular to the shear direction, as shown in the schematic illustration (Figure 3, top). We have several diffraction spots on the meridian arising from the parallel stacks of nanocylinders when viewed from X and Y directions (Figure 3, parts a and b), whereas the hexagonally symmetrical diffraction is observed when viewed from Z direction (Figure 3c). Parts a−c of Figure 3 clearly indicate that the PCL nanocylinder is preferentially oriented parallel to the shear direction applied to PCL−PS. We cleaved the block junction by irradiating UV after confirming the orientation of nanocylinders. It was completely preserved in PCL/PS, because the 2D- SAXS patterns of PCL/PS observed from each direction (Figure 3d−f) were almost identical with those of PCL−PS (Figure 3a−c). Therefore, it is possible to investigate crystal orientation of PCL homopolymers and PCL blocks confined in the nanocylinders with identical geometry as a function of crystallization temperature T_c.

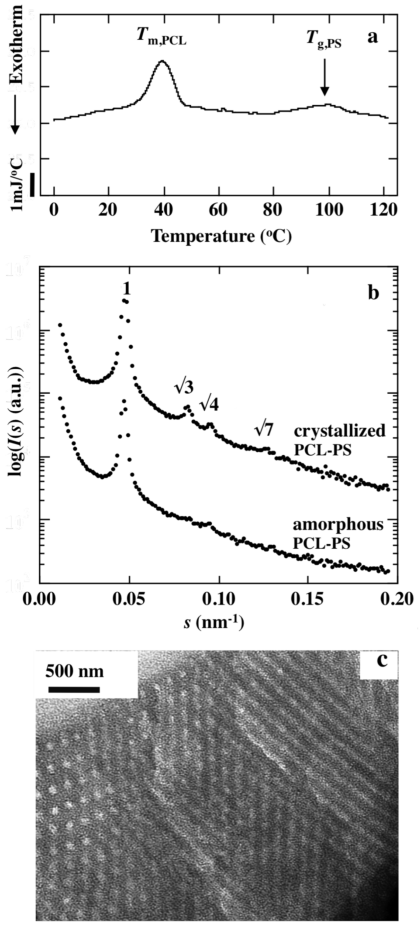

Figure 2. (a) DSC curve of PCL−PS, crystallized at −60 °C for 4 h, during heating at 20 °C/min from 0 °C into 120 °C. The endothermic peak appearing at ca. 40 °C corresponds to melting of PCL blocks and the change in the baseline (indicated by an arrow) at ca. 100 °C to glass transition of PS blocks. (b) 1D-SAXS curves of crystallized PCL−PS and amorphous PCL−PS. The difference in electron density between PS and crystallized PCL is significantly larger than that between PS and amorphous PCL, so that the higher-order peaks can be clearly observed for crystallized PCL−PS. (c) TEM picture of PCL−PS crystallized at −60 °C for 4 h.

In summary, PCL−PS used in this study formed the cylindrical microdomain structure with the PCL cylinder and PS matrix (1D-SAXS and TEM results), and the PCL nanocylinders could be preferentially oriented parallel to the shear direction (2D-SAXS results). Because $T_{g,PS}$ (~100 °C) was sufficiently higher than $T_{m,PCL}$ (~40 °C), PCL and PS homopolymers in PCL/PS did not take macrophase separation at the temperatures below $T_{g,PS}$. Therefore, it is possible to crystallize and melt PCL homopolymers repeatedly within the nanocylinders surrounded by PS matrices.

3.2. Orientation of PCL Lamellar Crystals. The PCL blocks in PCL−PS and PCL homopolymers in PCL/PS both confined in the oriented nanocylinders were crystallized at several temperatures ranging from −40 to −60 °C, and orientation of PCL lamellar crystals was investigated using 2D-WAXD. Figure 4 shows the typical 2D-WAXD patterns observed from the *X* direction (a, c) and the *Z* direction (b, d) for PCL−PS crystallized at −44 °C (a, b) and PCL/PS at −40 °C (c, d), where the 2D-WAXD pattern observed from the *Y* direction is omitted because it should be the same in principle to that observed from the *X* direction. We find two clear diffractions in every WAXD pattern in addition to the amorphous halo arising from the amorphous components

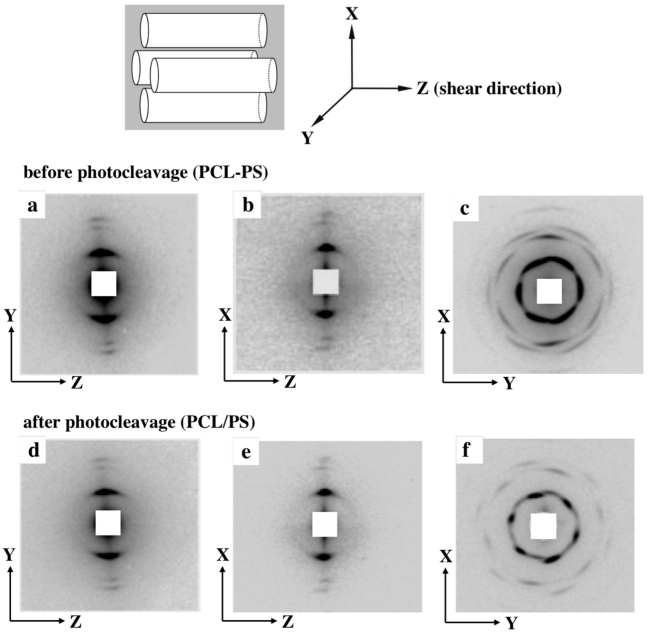

Figure 3. 2D-SAXS patterns observed from X direction (a, d), Y direction (b, e), and Z direction (c, f) for PCL−PS (upper panels) and PCL/PS (lower panels) both crystallized at −60 °C for 4 h. The definition of each direction against the shear direction is shown in the illustration (top).

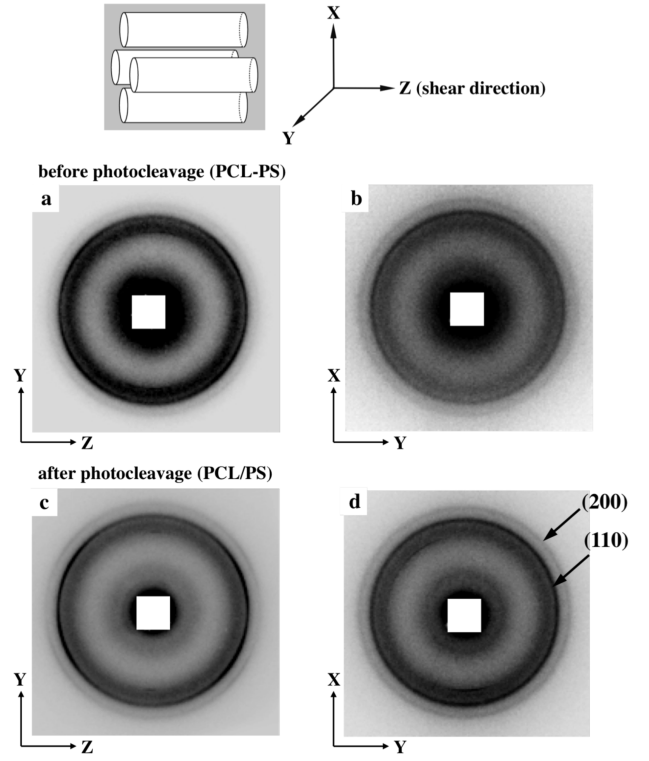

Figure 4. 2D-WAXD patterns observed from the *X* direction (a, c) and the *Z* direction (b, d) for PCL−PS crystallized at −44 °C (a, b) and PCL/PS crystallized at −40 °C (c, d). The definition of each direction against the shear direction is shown in the illustration (top).

existing in the system (PS and uncrystallized PCL). The X-ray crystallographic analysis of bulk PCL homopolymers [36] has revealed that the PCL crystal gives the strongest (110) diffraction at $2\theta = 21.41°$ and the second strongest (200) diffraction at $2\theta = 23.76°$. It is also reported that the intensity of these two diffractions is extremely stronger than

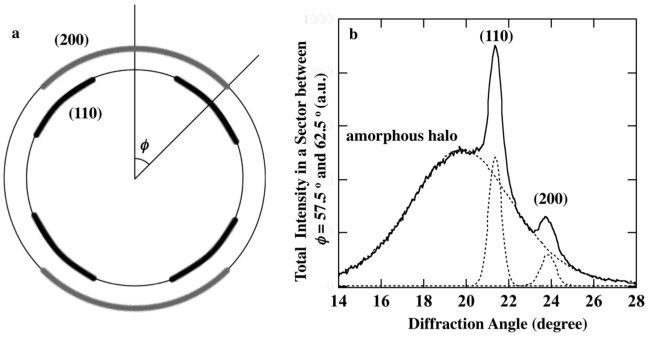

Figure 5. (a) Schematic 2D-WAXD pattern corresponding to Figure 4, parts a and c. (b) Total intensity in a sector between $\phi = 57.5°$ and 62.5° plotted against the diffraction angle 2θ to show the separation of the (110) and (200) diffractions (dotted peaks) from the amorphous halo.

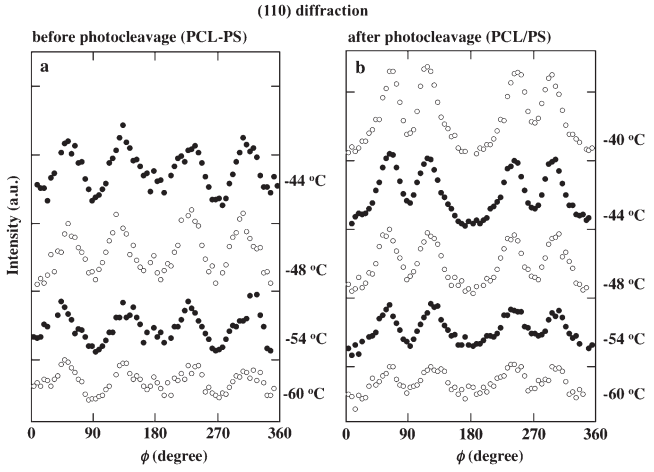

Figure 6. Integrated intensities of the (110) diffraction plotted against azimuthal angle ϕ for PCL−PS (a) and PCL/PS (b) crystallized at selected temperatures indicated. The plots are successively shifted upward for legibility.

that of other diffractions, so that weak diffractions cannot be detected when the total crystallinity of PCL chains is small, as is the case for our copolymer. Therefore, we can easily assign the (110) and (200) diffractions, as shown in Figure 4d.

We find from Figure 4 that the (110) diffraction intensity depends significantly on azimuthal angle ϕ when observed from X direction (a, c), whereas it is almost isotropic and independent of ϕ when observed from Z direction (b, d). Figure 5a shows the schematic illustration showing the typical WAXD pattern of Figure 4, parts a and c, where we emphasize the (110) and (200) diffractions by the thick arcs. In order to intuitively understand the one-dimensional diffraction profile, the total intensity in a sector between $\phi = 57.5°$ and 62.5° is radially plotted against diffraction angle 2θ in Figure 5b. We can find from Figure 5b that it is necessary to subtract the large intensity contribution arising from the amorphous halo for evaluating the (110) and (200) diffraction intensities. Therefore, we analytically performed the peak separation using a software PEAKFIT (Systat Software Ltd.) assuming the Gaussian function for each diffraction peak and the amorphous halo to successfully evaluate the intensity profiles of the (110) and (200) diffractions (dotted peaks in Figure 5b) as a function of ϕ at each T_c.

Figure 6 shows the integrated intensity of the (110) diffraction observed from X direction, *i.e.*, peak area under the (110) diffraction shown in Figure 5b, plotted against ϕ for PCL−PS (a) and PCL/PS (b) crystallized at the selected

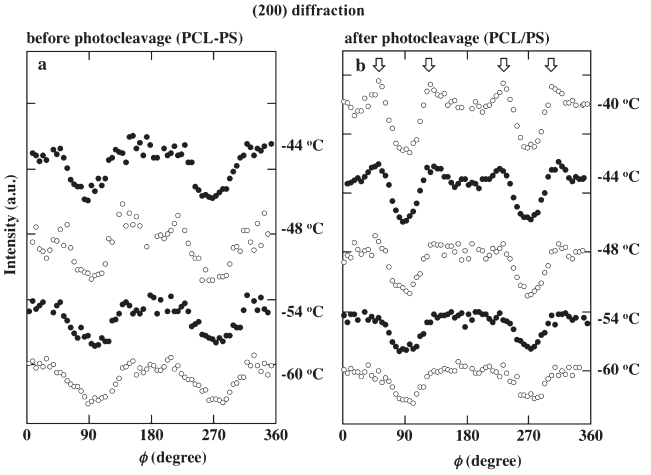

Figure 7. Integrated intensities of the (200) diffraction plotted against azimuthal angle ϕ for PCL−PS (a) and PCL/PS (b) crystallized at the selected temperatures indicated.

T_c indicated. We can find four distinct peaks at off-axis regions, the positions of which are almost independent of T_c. It is important to point out that these peaks do not imply that all PCL lamellar crystals orient perfectly to a specific direction, but some crystals take random orientation because a small and constant diffraction is detected at every ϕ in addition to the extra intensity at fixed ϕ. It is also found from Figure 6 that the peak intensity increases remarkably with increasing T_c for PCL/PS (Figure 6b), whereas it changes slightly for PCL−PS (Figure 6a). It should be noted that we could not obtain the WAXD pattern for PCL−PS at $T_c = -40$ °C because the PCL block did not crystallize within our experimental time (= 2 days). Figure 7 shows the integrated intensity of the (200) diffraction shown in Figure 5b plotted against ϕ for PCL−PS (a) and PCL/PS (b). Though these (200) diffraction profiles are moderately scattered due to the weaker intensity, they have two diffuse peaks centered at $\phi = 0$ and 180° and do not change significantly with changing T_c except for those of PCL/PS at −40 and −44 °C, which we will discuss later.

If we assume that the *b* axis of the unit cell for PCL crystals (fast growth axis[37]) is oriented parallel to the long axis of nanocylinders, which means the chain stem (PCL lamella normal) is perpendicular to the cylinder axis, we can expect from the unit cell dimension of PCL crystals[36] that the (110) diffraction will appear at $\phi = 58°$, 122°, 238°, and 302° and the (200) diffraction at $\phi = 0°$ and 180°. These expected ϕ values of the (110) and (200) diffractions agree satisfactorily with the positions of experimental diffraction peaks shown in Figures 6 and 7. In addition, the assumed crystal orientation in nanocylinders gives the isotropic intensity of the (100) and (200) diffractions when viewed from the *Z* direction, which also agrees with the experimental results shown in Figure 4, parts b and d. This type of crystal orientation is reported for crystallization of some block chains confined in nanocylinders,[14,15] for which it is concluded that the lamellar crystals grow long when the fast growth direction (*b* axis) coincides with the cylinder axis. The broadening of the (110) and (200) diffraction peaks shown in Figures 6 and 7 should be basically related to the degree of crystal orientation *f* in nanocylinders in addition to the slight misalignment of nanocylinders against Z direction. We will evaluate *f* as a function of T_c for PCL−PS and PS/PS in the next section.

In summary, the WAXD patterns observed from *X* and *Z* directions indicated that the PCL lamellar crystals oriented such that the *b* axis of the PCL unit cell (fast growth axis) was

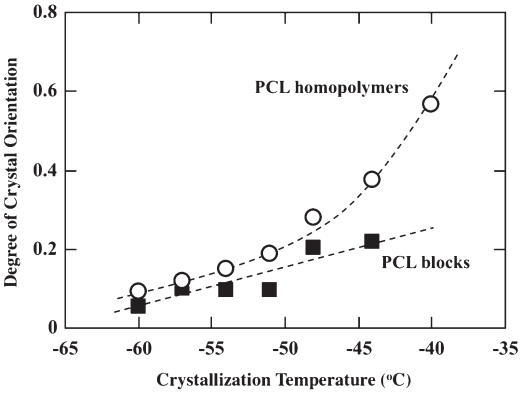

Figure 8. Degree of crystal orientation plotted against crystallization temperature for PCL blocks in PCL−PS (closed square) and PCL homopolymers in PCL/PS (open circle).

parallel to the long axis of nanocylinders both for PCL−PS and PCL/PS irrespective of T_c. The (110) diffraction intensity when plotted against ϕ (Figure 6) depended significantly on T_c for PCL/PS but not for PCL−PS, which will be intimately related to the degree of crystal orientation in nanocylinders.

3.3. T_c Dependence of Crystal Orientation. Several methods are used to evaluate the degree of crystal orientation f from the ϕ dependence of WAXD profiles [38]. Here, we evaluate f from the second-order moment of the orientation distribution function using the (110) diffraction profile,

$$f = \frac{k^{-1}\langle \cos^2 \phi \rangle - 1}{k^{-1} - 1} \tag{3}$$

where k represents $\langle \cos^2 \phi \rangle$ at random orientation (usually $k = {}^1/_3$), and $\langle \cos^2 \phi \rangle$ of the present case is calculated by

$$\langle \cos^2 \phi \rangle = \frac{\int_0^{\pi/2} I(\phi) \cos^2(\phi - \sigma) \sin(\phi - \sigma)\, d\phi}{\int_0^{\pi/2} I(\phi) \sin(\phi - \sigma)\, d\phi} \tag{4}$$

where $I(\phi)$ is the 1D intensity of the (110) diffraction shown in Figure 6 and σ is the azimuthal angle giving the maximum (110) diffraction between $\phi = 0$ and $\pi/2$. Actually, we first subtracted the constant intensity arising from a small unoriented component, then f was calculated at each quadrant, and finally four values were averaged together to evaluate f at each T_c for PCL−PS and PCL/PS. We also tried to evaluate f using the ϕ dependence of the (200) diffraction (Figure 7). However, these results included much scattering of data points owing to the weaker (200) diffraction, so that we present here the results obtained from the (110) diffraction profile. Figure 8 shows the T_c dependence of f for PCL blocks in PCL−PS (closed square) and PCL homopolymers in PCL/PS (open circle) calculated from eq 3. Though f is small and similar for both cases at lower T_c ($-60 \le T_c \le -54$ °C), it increases remarkably with increasing T_c for PCL homopolymers, indicating that crystal orientation is considerably improved at higher T_c. On the other hand, f increases slightly for PCL blocks, suggesting that T_c does not seriously affect the crystallization process and crystal orientation of PCL blocks.

The difference in the T_c dependence of f between PCL blocks and PCL homopolymers should be solely ascribed to the effect of chain confinement, that is, PCL blocks are tethered at the nanocylinder interface while PCL homopolymers are free. Figure 8 can be successfully explained in terms of above tethering effect of PCL chains together with the T_c dependence of crystal growth rate for each PCL chain. Crystallization necessarily requires the mobility of crystalline components to diffuse into the crystal growth front, and therefore the crystallization rate (growth rate) is higher for crystalline chains with larger mobility. When T_c is increased or the molecular weight of crystalline components is decreased, the chain mobility accelerates to yield the larger crystallization rate. This is the case for PCL homopolymers shown in Figure 8. That is, at the initial stage of crystallization, homogeneous nucleation occurs at some places in the nanocylinder and the PCL crystals grow to every direction. However, the crystal growth rate is extremely limited at lower T_c owing to the small mobility of PCL chains by the proximity of glass transition. As a result, several immature lamellar crystals yield in the nanocylinder, showing a small f at lower T_c. At higher T_c, on the other hand, crystal growth continues for the lamellar crystals whose fast growth axis (b axis) is parallel to the cylinder axis to yield the developed crystals preferentially oriented parallel to the cylinder axis, resulting in a progressively increasing f. On the basis of above discussion, crystal orientation is schematically depicted in Figure 9 for PCL homopolymers crystallized at low T_c (∼−60 °C) and high T_c (∼−40 °C), where the lamellar crystals are immature at $T_c = -60$ °C and their distribution of crystal orientation is larger by tilting vertically and horizontally, whereas the average tilting reduces considerably by the formation of large lamellar crystals at $T_c = -40$ °C.

In the case of PCL blocks, the conformation and mobility are considerably restricted owing to the tethering effect compared with those of PCL homopolymers. As a result, the mobility of PCL blocks does not increase significantly with increasing T_c, and eventually many less-oriented lamellar crystals appear in nanocylinders irrespective of T_c. Therefore, f is relatively low for PCL blocks and does not increase extremely with increasing T_c. The intuitive picture for crystal orientation of PCL blocks at every T_c is similar to that of PCL homopolymers at $T_c = -60$ °C (upper illustration in Figure 9). It is worth noting that the angular distribution of the (200) diffraction centered at $\phi = 0°$ and 180° (Figure 7) seems to be larger compared with the (110) diffraction appearing at the off-axis regions (Figure 6). In addition, we find faint peaks at $\phi = 52$, 128, 232, and 308° only for PCL homopolymers crystallized at -40 and -44 °C (indicated by arrows in Figure 7b). These facts suggest that a small amount of PCL lamellar crystals with other preferential orientation (which gives the four-spot (200) diffraction) might exist in PCL/PS at higher T_c in addition to regular orientation described above. However, such crystal orientation cannot be uniquely determined only from the (110) and (200) diffraction profiles.

In summary, we found from the ϕ dependence of the (110) diffraction intensity that crystal orientation of PCL homopolymers confined in nanocylinders increased remarkably with increasing T_c and that of PCL blocks changed slightly, resulting in a large difference in f between PCL blocks and PCL homopolymers at higher T_c (≥ -45 °C). It is because the PCL chain confinement (or tethering effect imposed on PCL blocks) yielded the significant difference in the T_c dependence of chain mobility during isothermal crystallization.

3.4. Comparison with Other Experimental Results. Here, we compare our experimental results obtained for PCL−PS and PCL/PS with those for other systems and the prediction of computer simulation. Quiram et al.[13,14] and Huang et al.[15,16] have investigated crystal orientation of block chains confined in nanocylinders provided by microphase separation of molten crystalline−amorphous diblocks as a function of crystalline temperature T_c. They found that crystal orientation depended significantly on T_c: at lower T_c, the orientation was almost random, while it was gradually

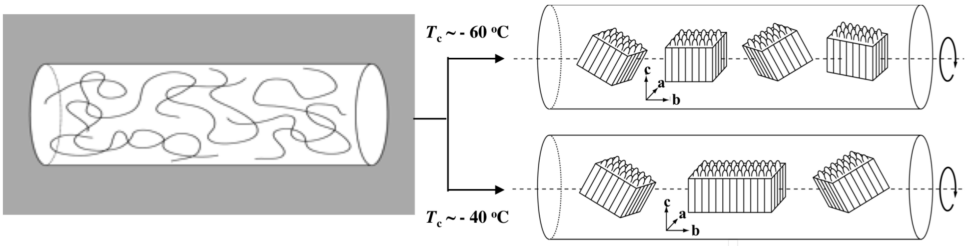

Figure 9. Schematic illustration showing the difference in crystal orientation in the nanocylinders between PCL homopolymers crystallized at −60 °C (a) and −40 °C (b).

improved with increasing T_c, and finally the chain stem (*c* axis of crystal unit cells) was preferentially oriented perpendicular to the cylinder axis. Quiram et al.[14] explained this orientation change in terms of the crystal growth rate (or diffusion rate) of crystalline blocks. That is, crystal orientation in nanocylinders was accelerated with increasing the diffusion rate of crystalline blocks, *i.e.*, with increasing T_c or decreasing molecular weight, to result in preferential orientation of the *b* axis (fast growth axis) along the cylinder axis. Our results for crystal orientation of PCL blocks and PCL homopolymers shown in Figure 8 agree qualitatively with this interpretation. The mobility of PCL homopolymers at lower T_c (≤- 54 °C) is extremely small and similar to that of PCL blocks resulting in a similar small *f*. However, it is easily expected that the mobility of PCL homopolymers will increase considerably with increasing T_c compared with that of PCL blocks, so that *f* of PCL homopolymers will increase remarkably at higher T_c (≥−50 °C). Therefore, the experimental results shown in Figure 8 for PCL−PS and PCL/PS are consistent with the interpretation that crystal orientation in nanocylinders is mainly controlled by the diffusion rate of crystalline chains at each T_c.

Crystal orientation of homopolymers confined in nanocylinders has been recently investigated using anodic aluminum oxide (AAO).[17−20] AAO contains homogeneous nanopores (or nanocylinders) inside, and the pore diameter can be easily controlled ranging from 15 to 220 nm.[18] All results showed that the chain stem of crystallized homopolymers was perpendicular to the cylinder axis and also that the melting temperature and crystallinity depended significantly on the pore diameter; the crystallinity decreased with decreasing the diameter. This result agrees qualitatively with ours when we compare the result of PCL/PS with that of PVL/PS previously reported.[25] The diameter of nanocylinders in PVL/PS is 15.7 nm and that in PCL/PS is 13.0 nm, and the melting enthalpy of PVL homopolymers crystallized at −49 °C is $\Delta H_{PVL} \sim 45$ J/g and that of PCL homopolymers at −48 °C is $\Delta H_{PCL} \sim 40$ J/g. If we assume that the heat of fusion for perfect PVL crystals, which is not available in the literature, is given by the interpolation between those of perfect PCL crystals ($\Delta H_{PCL} = 135$ J/g[28]) and poly(β-propiolactone) (PPL) crystals ($\Delta H_{PPL} = 119$ J/g[28,39]), the crystallinity of PVL is ca. 17% higher than that of PCL. This difference in crystallinity is moderately large when we compare it with the result of crystalline homopolymers confined in AAO nanopores (78% increase in crystallinity when the pore diameter changes from 15 to 110 nm[18]), because the difference in diameter of PCL and PVL nanocylinders is only 20%. Therefore, all results for homopolymer crystallization confined in AAO nanopores, i.e., *c*-axis orientation perpendicular to the cylinder axis and the change in crystallinity with changing the pore diameter, are consistent with our results for PCL and PVL homopolymers confined in nanocylinders. It should be noted that the difference in crystallinity between PVL and PCL blocks is extremely large; $\Delta H_{PVL} \sim 41$ J/g at $T_c = -49$ °C and $\Delta H_{PCL} \sim 17$ J/g at $T_c = -48$ °C, which corresponds to the 250% increase of crystallinity for PVL blocks.

Finally, we compare our results with the prediction of computer simulation.[21−24] Hu et al., for example, investigated the time evolution of crystal orientation for crystalline blocks and homopolymers both confined in spherical or cylindrical nanodomains using dynamic Monte Carlo simulation. The chain stem was preferentially oriented perpendicular to the cylinder axis during isothermal crystallization of crystalline blocks, and it was practically preserved after crystallization. This prediction of final crystal orientation is quantitatively consistent with our results of PCL blocks in PCL−PS. However, they predicted that parallel orientation transiently appeared at the early stage of isothermal crystallization for homopolymers, then the orientation gradually changed with increasing crystallization time, and finally the perpendicular orientation prevailed in the system. Though we did not pursue the time evolution of crystal orientation during isothermal crystallization of PCL homopolymers in the present study, final crystal orientation of PCL homopolymers is also consistent with the prediction of computer simulation made by Hu et al.

In summary, the previous experimental results for crystal orientation of crystalline blocks and homopolymers confined in nanocylinders, i.e., crystalline blocks in cylindrical microdomain structure and crystalline homopolymers in AAO nanopores, and the prediction of computer simulation for block and homopolymer crystallization confined in nanocylinders, all are consistent with the experimental results reported here for PCL−PS and PCL/PS. The large difference in the degree of crystal orientation at higher T_c between PCL homopolymers and PCL blocks provides important information about the effect of chain tethering on the isothermal crystallization mechanism.

4. Conclusions

We have investigated crystal orientation of poly(ε-caprolactone) (PCL) homopolymers and PCL blocks both confined in the nanocylinders with identical geometry surrounded by polystyrene (PS) matrices as a function of crystallization temperature T_c. The PCL-*b*-PS diblock copolymer with a photocleavage *o*-nitrobenzyl group between two blocks was synthesized, and the block junction was successfully cleaved by UV radiation to prepare PCL homopolymers confined in nanocylinders originally formed by microphase separation of PCL-*b*-PS. The nanocylinder could be preferentially oriented in the sample using the rotational shear in order to investigate crystal orientation of PCL chains existing within it. It was found that the *b* axis of the unit cell of PCL crystals was preferentially oriented parallel to the long axis of nanocylinders both for PCL homopolymers and PCL blocks. However, the degree of crystal orientation increased remarkably with increasing T_c for PCL homopolymers, whereas it improved

slightly for PCL blocks. This difference will arise from the fact that the restricted mobility of PCL blocks with one-end tethered at the nanocylinder interface suppresses the favorable crystal growth of PCL blocks during isothermal crystallization at higher T_c. Our experimental results presented here are consistent with those of crystalline blocks confined in cylindrical microdomain structure and crystalline homopolymers confined in AAO nanopores, and also with the prediction of computer simulation.

Acknowledgment. We appreciate Mr. J. Koki, Center for Advanced Materials Analysis, Tokyo Institute of Technology, for TEM observations. The 1D-SAXS measurement has been performed under the approval of Photon Factory Advisory Committee (No. 2008G031)

References and Notes

(1) Hamley, I. W.; Fairclough, J. P. A.; Terrill, N. J.; Ryan, A. J.; Lipic, P. M.; Bates, F. S.; Andrews, E. T. *Macromolecules* **1996**, *29*, 8835.
(2) Nojima, S.; Tanaka, H.; Rohadi, A.; Sasaki, S. *Polymer* **1998**, *39*, 1727.
(3) Weimann, P. A.; Hajduk, D. A.; Chu, C.; Chaffin, K. A.; Brodil, J. C.; Bates, F. S. *J. Polym. Sci.* **1999**, *B37*, 2053.
(4) Loo, Y. L.; Register, R. A.; Ryan, A. J.; Dee, G. T. *Macromolecules* **2001**, *34*, 8968.
(5) Loo, Y. L.; Register, R. A.; Ryan, A. J. *Macromolecules* **2002**, *35*, 2365.
(6) Nojima, S.; Toei, M.; Hara, S.; Tanimoto, S.; Sasaki, S. *Polymer* **2002**, *43*, 4087.
(7) Muller, A. J.; Balsamo, V.; Arnal, M. L.; Jakob, T.; Schmalz, H.; Abetz, V. *Macromolecules* **2002**, *35*, 3048.
(8) Zhu, L.; Huang, P.; Chen, W. Y.; Ge, Q.; Quirk, R. P.; Cheng, S. Z. D.; Thomas, E. L.; Lotz, B.; Hsiao, B. S.; Yeh, F.; Liu, L. *Macromolecules* **2002**, *35*, 3553.
(9) Takeshita, H.; Ishii, N.; Araki, C.; Miya, M.; Takenaka, K.; Shiomi, T. *J. Polym. Sci.* **2004**, *B42*, 4199.
(10) Muller, A. J.; Balsamo, V.; Arnal, M. L. *Adv. Polym. Sci.* **2005**, *190*, 1.
(11) Lorenzo, A. T.; Arnal, M. L.; Muller, A. J.; Fierro, A. B.; Abetz, V. *Eur. Polym. J.* **2006**, *42*, 516.
(12) Sun, Y. S.; Chung, T. M.; Li, Y. J.; Ho, R. M.; Ko, B. T.; Jeng, U. S. *Macromolecules* **2007**, *40*, 6778.
(13) Quiram, D. J.; Register, R. A.; Marchand, G. R. *Macromolecules* **1997**, *30*, 4551.
(14) Quiram, D. J.; Register, R. A.; Marchand, G. R.; Adamson, D. H. *Macromolecules* **1998**, *31*, 4891.
(15) Huang, P.; Zhu, L.; Cheng, S. Z. D.; Ge, Q.; Quirk, R. P.; Thomas, E. L.; Lotz, B.; Hsiao, B. S.; Liu, L.; Yeh, F. *Macromolecules* **2001**, *34*, 6649.
(16) Huang, P.; Guo, Y.; Quirk, R. P.; Ruan, J.; Lotz, B.; Thomas, E. L.; Hsiao, B. S.; Avila-Orta, C. A.; Sics, I.; Cheng, S. Z. D. *Polymer* **2006**, *47*, 5457.
(17) Steinhart, M.; Goring, P.; Dernaika, H.; Prabhukaran, M.; Gosele, U.; Hempel, E.; Thurn-Albrecht, T. *Phys. Rev. Lett.* **2006**, *97*, 027801.
(18) Shin, K.; Woo, E.; Jeong, Y. G.; Kim, C.; Huh, J.; Kim, K. W. *Macromolecules* **2007**, *40*, 6617.
(19) Wu, H.; Wang, W.; Huang, Y.; Wang, C.; Su, Z. *Macromolecules* **2008**, *41*, 7755.
(20) Wu, H.; Wang, W.; Huang, Y.; Su, Z. *Macromol. Rapid Commun.* **2009**, *30*, 194.
(21) Wang, M.; Hu, W.; Ma, Y.; Ma, Y. Q. *J. Chem. Phys.* **2006**, *124*, 244901.
(22) Miura, T.; Mikami, M. *Phys. Rev. E* **2007**, *75*, 031804.
(23) Qian, Y.; Cai, T.; Hu, W. *Macromolecules* **2008**, *41*, 7625.
(24) Cai, T.; Qian, Y.; Ma, Y.; Ren, Y.; Hu, W. *Macromolecules* **2009**, *42*, 3381.
(25) Nojima, S.; Ohguma, Y.; Namiki, S.; Ishizone, T.; Yamaguchi, K. *Macromolecules* **2008**, *41*, 1915.
(26) Yamaguchi, K.; Kitabatake, T.; Izawa, M.; Fujiwara, T.; Nishimura, H.; Futami, T. *Chem. Lett.* **2000**, *29*, 228.
(27) Richardson, M. J.; Savill, N. G. *Polymer* **1977**, *18*, 3.
(28) Crescenzi, V.; Manzini, G.; Calzolari, G.; Borri, C. *Eur. Polym. J.* **1972**, *8*, 449.
(29) Trent, J. S.; Scheinbeim, J. I.; Couchman, P. R. *Macromolecules* **1983**, *16*, 589.
(30) Nojima, S.; Hashizume, K.; Rohadi, A.; Sasaki, S. *Polymer* **1997**, *38*, 2711.
(31) Nojima, S.; Kikuchi, N.; Rohadi, A.; Tanimoto, S.; Sasaki, S. *Macromolecules* **1999**, *32*, 3727.
(32) Nojima, S.; Akutsu, Y.; Akaba, M.; Tanimoto, S. *Polymer* **2005**, *46*, 4060.
(33) Nojima, S.; Kiji, T.; Ohguma, Y. *Macromolecules* **2007**, *40*, 7566.
(34) Hamley, I. W. *The Physics of Block Copolymers*; Oxford Univ. Press: New York, 1998.
(35) Loo, Y. L.; Register, R. A. In *Developments in Block Copolymer Science and Technology*; Hamley, I. W., Ed., John Wiley & Sons: Chichester, U.K., 2004.
(36) Chatani, Y.; Okita, Y.; Tadokoro, H.; Yamashita., Y. *Polym. J.* **1970**, *1*, 555.
(37) Beekmans, L. G. M.; Vancso, G. J. *Polymer* **2000**, *41*, 8975.
(38) Miyazaki, T.; Hoshiko, A.; Akasaka, M.; Sakai, M.; Takeda, Y.; Sakurai, S. *Macromolecules* **2007**, *40*, 8277.
(39) Nojima, S.; Fukagawa, Y.; Ikeda, H. *Macromolecules* **2009**, *42*, 9515.